Final Research Results Supported by the KFAS International Scholar Exchange Fellowship Program, 2006-2007

Quantum Chaos in Deformed Microcavities

(Hỗn loạn lượng tử trong các hốc cộng hưởng vi mô biến dạng)

Ph.D. Truong Thi Anh Dao
(Trương Thị Anh Đào)

Vietnamese Academy of Science and Technology (VAST)

Host scholar : **Professor Kyung Won An**

Seoul National University

August 15, 2007

Abstract

One of the behaviours to reach studying the quantum states is to consider them at the boundary of clasical mechanics whereas the applicability of clasical mechanics theory.

Quantum chaos arising from semiclassical models and the classical limit of a quantum description may lead to a mechanical system with chaotic dynamics.

We propose the principle to build a deformed microcavity for reseach quantum properties in chaos medium to elucidate the interplay between wave and particle natures of light.

We have been used the deformed microcavity as a efficiency tool to study that chaos medium.

We have developed a chechnique for realizing a two dimensional quadupolar microcavity with its deformation variable from 0% to 20 % continuosly using a liquid jet ejected from concircular orifice. With this technique, we investigated the far field evolution depending on deformation parameter from regularity to chaos.

Tóm tắt nội dung công trình

Một trong những phương cách để đạt tới việc nghiên cứu các trạng thái lượng tử là xem xét chúng ở giới hạn của cơ học cổ điển mà ở đó ta có thể áp dụng được lý thuyết cơ học cổ điển.

Quantum chaos là được phát triển từ các mô hình bán cổ điển và giới hạn cổ điển của một mô tả lượng tử có thể dẫn tới một hệ với động học hổn loạn

Chúng tôi đề ra nguyên lý thiết lập một hốc cộng hưởng vi mô biến dạng để nghiên cứu các đặc tính lượng tử trong môi trường hỗn loạn để làm sáng tỏ tác động lẫn nhau giữa sóng và hạt.

Chúng tôi sử dụng hốc cộng hưởng vi mô biến dạng như là một công cụ hiệu quả để nghiên cứu môi trường hỗn loạn đó.

Chúng tôi phát triển một kỹ thuật để tìm hiểu một hốc cộng hưởng vi mô biến dạng bốn cạnh với độ biến dạng thay đổi liên tục từ 0% đến 22% sử dụng một dung dịch được bơm vào từ các ống không tròn . Với kỹ thuật này, chúng tôi đã nghiên cứu tiến trình trường- xa phụ thuộc lên các thông số biến dạng từ sự cân đối đến hỗn loạn.

1. Quantum chaos and its questions under investigation

Introduction

Quantum chaos attempts a synthesis of ideas from two active research fields: The study of optical microcavities, and the theory of dynamical systems whose classical phase space is partially chaotic. For its nonclassical counterpart, the quantummechanics of chaotic systems, termed in short “quantum chaos”, the situation is completely different. Quantum chaos at first sight seems to be the exclusive domain of theoricians. The situation gradually changed in the middle of the eighties, since when numerous experiments have been performed. The underlying ideas are very simple. It is essentially the mathematical apparatus that makes things difficult and often tends to obscure the physical background. Therefore the philosophy adopted here is to a strong accentuation of **billiard systems** for which a large number of experiments now exist. Since the uncertainty relation

$$\Delta x \Delta p \geq \frac{1}{2}\hbar \qquad (1.1)$$

prevents a precise determination of the initial conditions. This can best be illustrated for the propagation of a point- like particle in a box with infinitely high walls. For obvious reasons these systems are called billiards.

The billiard, though being conceptually simple, nevertheless exhibits the full complexity of nonlinear dynamics, including its quantum machanical aspects. Probably there is no essential aspect of quantum chaos which cannot be found in chaotic billiards. Quantum mechanics has now existed for more than 60 years and has probably become the best tested physical theory ever conceived. Quantum mechanics can handle not only the hydrogen atom which is classically integrable but also the classically nonintegrable helium atom. We may even ask whether there is anything like quantum chaos at all. The Schrodinger equation is a linear equation leaving no room for chaos. Today the term “quantum chaos“ is generally understood to comprise all problems concerning the quantum machanical behavior of classically chaotic systems. Quantum chaos is the study of no separable Schrodinger equations based on a knowledge of the underlying classical mechanics, which can be chaotic when the system is **non-integrable.**

Generally, resonances are long-lived quasi-bound states in an **open system** that arise due to interference, and they give rise to sharp variation in scattering phase shifts, cross sections, transmission coefficients, etc., as the incident wavelength is varied. An open system is characterized by the existence of propagating waves at large distance from the region where the quasi-bound states are formed.

Helmholz equation in billiard experiments

Let $x(0)=\left[x_1(0),....x_N(0)\right]$ be the vector of the dynamical variables at the time t = 0. At any later time t we may write x(t) as a function of the initial conditions and the time as

$$x(t)=F\left[x(0),t\right] \qquad (1.2)$$

If the initial conditions are infinitesimally

$$x_1(0)=x(0)+\xi(0), \qquad (1.3)$$

then at a later time t the dynamical variables develop according to

$$x_1(t)=F\left[x(0)+\xi(0),t\right]. \qquad (1.4)$$

The distance $\xi(t)=x_n(t)-x(t)$ between the two trajectories is obtained from Eqs.(1.2) and (1.4) in linear approximation as

$$\xi(t)=\left(\xi(0)\nabla\right)F\left[x(0),t\right], \qquad (1.5)$$

Written in components Eq. (1.5) reads

$$\xi_n(t)=\sum_n \frac{\partial F_n}{\partial x_m}\xi_m(0). \qquad (1.6)$$

The eigenvalues of the matrix $M=\left(\partial F_n/\partial x_m\right)$ determine the stability properties of the trajectory. If the module of all eigenvalues are smaller then one, the trajectory is stable, and all deviations from the initial trajectory will rapidly approach zero. If the modulus of at least one eigenvalue is larger than one, both trajectory will exponentially depart from each other even for infinitesimally small initial deviations.

Stationary solutions of the Schrodinger equation are obtained by separating the time dependence,

$$\psi_n(x,t)=\psi_n(x)e^{iw_nt}. \qquad (1.7)$$

we have

$$\left(\Delta+k_n{}^2\right)\psi_n(x)=0 \qquad (1.8)$$

where ω_n and k_n are connected via the dispersion relation

$$\omega_n = \frac{\hbar}{2m} k_n^{\ 2} \qquad (1.9)$$

Equation (1.8) is also obtained if we start with the wave equation

$$\left(\Delta - \frac{1}{c^2} \frac{\partial^2}{\partial t^2} \right) \psi = 0, \qquad (1.10)$$

where c is the wave velocity, and if we separate again the time dependence by means of the ansatz (1.7). In contrast to the quadratic dispersion relation (1.9) for the quantum mechanical case we now have the linear relation

$$\omega_n = c k_n \qquad (1.11)$$

between ω_n and k_n . It is exactly this correspondence between the stationary Schrodinger equation and the stationary wave equation, also called the **Helmholz equation**, which has been used in many billiard experiments to study quantum chaotic problems using wave analogue systems.

Integrable systems

We have learnt that random matrix theory is perfectly able to explain the universal properties of the spectra of chaotic systems. On the one hand it is very satisfactory that one single theory can cope with such a variety of systems as nuclei , mesoscopic structures, or microwave billiards, on the other hand this is a bit disappointing. If there is no possibility of discriminating between the spectra of a nucleus and a quantum dot , then there is little hope of learning anything of relevance about it.

Fortunately, random matrix theory is only one side of the coin. The spectral level dynamics where bouncing balls disturbed the otherwise universal Gaussian velocity distribution. Another example is the scarring phenomenon observed in many wave functions. Here obviously closed classical orbits have left their fingerprints in the amplitude patterns. We cannot expect that the universal random matrix theory can correctly account for individual features such as periodic orbits.

As we know from the correspondence principle, in the semiclassical limit of high quantum numbers. We have already discussed this connection for a particle in a one- dimensional box. The general case has been treated by M.Gutzwiller [17,18]. In there have two part : Trace formula, establishing a correspondence between the quantum mechanical spectrum and the periodic orbits of a system and a number of applications of the trace formula will be examined.

In most isolated mechanical systems occurring in nature, the only conserved quantity is the total energy. As soon as there is more than one degree of freedom, it becomes very difficult to solve the equations of motion under these circumstances. Practically all textbook examples for motion in more than one dimension therefore belong to a special class of systems which axe called *integrable* because the trajectory can be found by a set of quadratures.

Assume that in addition to the Hamiltonian H, let found another function $K(\bar{x})$ of the phase space variables that is also conserved, i.e. $\{K, H\} = 0$. The system is integrable if there are N conserved quantities like H and K which are also pair wise independent and have vanishing Poisson bracket with each other. Let explore this situation for the special case of $N = 2$. Independence of H and K means that we require their gradients to be linearly independent,

$$\vec{\nabla}_x H \neq \alpha \vec{\nabla}_x K \qquad (1.12)$$

every where except at isolated points in the four-dimensional phase space. The trajectory is constrained by the two equations $H\{x\}=E$ and $K\{x\}=const$, and therefore lies on a 2D surface F. Any point on that surface can serve as the initial condition for a unique trajectory consistent with the conservation laws, and the resulting set of trajectories defines a new vector field: the projection of $\frac{d}{dt}\left(\bar{x}\right)$ onto the local tangent plane of F. This 2D field covers the whole surface, and it is nonzero everywhere provided $\frac{d}{dt}\left(\bar{x}\right) \neq 0$. The latter condition is assumed to be valid in the cases of interest here, as is done the textbook by Arnol'd [19]

In order for F to be covered by an everywhere nonvanishing vector field, its topology must be that of a torus. One can easily visualize that a sphere does not admit such a field . In fact this topology introducing further handles on the torus will again make it impossible to avoid points of vanishing field.

The generalization of the above arguments to more than two degrees of freedom is that the trajectory will move on an N-dimensional torus in the 2N-dimensional phase space. However, the case $N = 2$ is of particular interest to us.

Concerning the assumption that the vector field on F is nonvanishing, it should be pointed out that there are counter-examples, namely the rational polygon billiards [20], which consist of flat billiards bounded by straight line segments enclosing an angle which is a rational multiple of π. These systems are called *pseudo-integrable*, and the motion of a trajectory is confined to a two-dimensional manifold in phase space. However, the possibility of (classical) "beam splitting" at sharp corners implies that singularities of the above vector field can occur. As a result, the surface F is a multi-handled sphere, which becomes so complicated that the system shows some properties commonly associated with nonintegrable dynamics, as for example level repulsion in the quantum mechanical spectrum.

The long *lifetime* of photons in a laser resonator is what makes it possible to obtain coherent stimulated emission. The *sharply peaked* wavelength-dependent transmission of a Fabry - Perot interferometer is the basis of high resolution spectroscopy. The characteristic wavelengths λ at which resonances occur, as well as their lifetimes τ, are device-specific. In optics, one uses the Q factor as a figure of merit for the resonator, where $Q \equiv \omega\,\tau$, $\omega \equiv \Pi C/\Lambda$
When there exist as many conservation laws as there are degrees of freedom, a system is called **integrable**. The complexity of the problem is greatly increased in *non-integrable* systems, where it becomes impossible to reduce the wave equation to a collection of separate first-order differential equations. Meanwhile in optics, a theory of **nonintegrable** resonators only existed in the form of perturbation approaches [1] where the breaking of symmetries was treated in the limit where it causes only a small correction to the symmetric solutions.

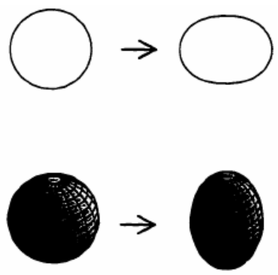

Figure 1.1. Integrable shapes (left) in two and three dimensions and their non-integrable deformed counterparts [2]

It has recently been realized [2] that nonperturbative effects may in fact be useful in device applications, and one therefore desires models that could make predictions and provide explanations for phenomena observed in strongly non-separable wave equations.

Classical ray dynamics

The ray dynamics analysis is facilitated by the axial symmetry of the droplets which implies (in the language of particle trajectories) that the z component of angular momentum, $\boldsymbol{L_z}$ is conserved. At any given $\boldsymbol{L_z}$ and total energy E, the equations of motion thus have only two degrees of freedom, just as in the deformed cylinder. This becomes explicit in cylindrical coordinates $\boldsymbol{\rho}$, $\boldsymbol{\varphi}$, $\boldsymbol{z}$ where one has

$$E = \frac{1}{2} m \left(\dot{\rho}^2 + \dot{z}^2 \right) + \frac{L_z^2}{2m\rho^2} \qquad (1.13)$$

Let us look at the dynamics projected into the 2D (p, *z)* coordinate system.

Each specula reflection causes a discontinuous change in $\dot{\rho}$ and $\dot{z}$ *;* however the angular velocity $\dot{\phi}$ remains unchanged because the normal to the surface of an axisymmetric cavity is always perpendicular to the *Φ* direction. Thus a 3D specula reflection simply reverses the normal component of the 2D projected velocity $\left(\dot{\rho}, \dot{z}\right)$ and reflections are also specula in the projected coordinates. Reflections occur whenever the trajectory $\rho(z)$ intersects the boundary curve $\rho_b(z)$. Between reflections the particle motion is free, $\dot{z}$ = const, and Eq. (1.13) can be integrated to find $\rho(t)$. It can be shown that $\rho^2(z)$ describes a parabola whose vertex is the point of closest approach to the z-axis and whose intersections with the squared boundary curve $\rho_b^2(z)$ are the collision points. The curved trajectories in the z-ρ-plane between specula bounces are to be contrasted with the straight paths in conventional 2D billiards where the centrifugal potential $L^2_z/(2m\rho^2)$ is absent.

The resulting dynamics introduced dimensionless variables in Eq. (1.13) by setting $E = 1/2$ and $m = 1$**.** Then one has

$$1 = \dot{\rho}^2 + \dot{z}^2 + \frac{L_z^2}{\rho^2} \qquad (1.14)$$

where $0 \le L_z \le \rho_b(z_{max})$ is the maximum distance from the z-axis is $\rho_b(z_{max})$**.** To simplify notation , assume that the droplets have their widest transverse cross-section in the equatorial plane, i.e. $z_{max} = 0$**.** Again the escape condition is simply $\sin\chi < \sin\chi_c$ where $\sin\chi$ is *the* angle of incidence with respect to the surface normal n at the reflection point. This is not the same as the normal angle in the *ρ* - z-plane, as can be seen by considering a trajectory reflecting entirely in the equatorial plane at nonzero $\sin\chi$; its apparent angle of incidence in the *ρ* — z-plane will be zero. The angle in the *p* — z-plane is then given by

$$\cos\chi_{\rho z} = \cos\chi / \sqrt{\dot{\rho}^2 + \dot{z}^2} \quad (1.15)$$

It is convenient in the plotting of Poincare sections to use as variables the polar angle *θ* and the 3D $\sin\chi$ at each reflection since in these coordinates the escape condition is still satisfied along a horizontal straight line.

At nonzero L_z certain regions of the SOS are forbidden due to the L_z angular momentum barrier (e.g. a ray reaching the pole *(θ* = 0) must have L_z =0). For the allowed bounce coordinates *θ,* $\sin\chi$ one finds the inequality $\sin\chi > L_z/\rho_b(z(\theta))$, where $z(\theta) = \tau_b(\theta)\sin\theta$. Before discussing ray escape in the deformed droplets it is important to note that as we proceed from higher to lower L_z in addition to the excluded regions of the SOS decreasing (because the angular momentum barrier becomes weaker) the degree of chaos grows rapidly. There is actually no visible chaos and a mostly chaotic SOS for $L_z = 0$ *for a droplet of fixed deformation.* The reason for this is that high L_z trajectories are confined near the equator and a cross-section of the droplet at the equator is perfectly circular, i.e. high L_z orbits see an effective deformation which is much weaker than polar orbits ($L_z = 0$) which travel in the most deformed cross- section of the droplet. The effective deformation

$$\varepsilon_{eff} = \varepsilon\sqrt{1 - L_z^2 / \rho_b^2(0)} \qquad (1.16)$$

and tends to zero at the maximum allowed value of L_z. Thus as long as ε is large enough to induce classical Q-spoiling for the $L_z = 0$ orbits of interest, by looking at different L_z values for a fixed deformation one can study the classical Q- spoiling transition in a single ARC.

Note that there is an absolute minimum allowed $\boldsymbol{\sin\chi = \sin\chi_m}$ which occurs at the equator $(\theta = \pi/2)$ where ρ_b is maximal (i.e., $\sin\chi_m = L_z/\rho_b(0)$). This implies that classical ray escape is entirely forbidden due to the angular momentum barrier for values of $\boldsymbol{L_z > \rho_b(0)\sin\chi_c}$. As just noted these high L_Z modes are confined to orbits near the plane of the equator ; since classical escape is forbidden for these modes we always expect to find high-Q WG modes in the equatorial region of axially-symmetric deformed microspheres. Since this follows simply from L_z conservation it will be true in both the oblate and prolate shapes.

Proceeding now to lower L_z, we see that the angular momentum barrier has weakened enough that the allowed region of the SOS passes through $\boldsymbol{\sin\chi_c}$ and rays with this value of L_z can escape. However as before WG modes will be associated with rays starting at large $\boldsymbol{\sin\chi} \approx 0.9$ in this case. These rays are unable to reach $\boldsymbol{\sin\chi_c}$ due to remaining KAM curves.

Therefore high Q WG modes for this value of L_z as well. This situation persists all the way to $L_z = 0$ for deformations less than roughly 5% of the radius, so little Q-spoiling and approximately isotropic emission for smaller deformations than this.

However for the 50% deformation used reducing L_z a little more causes the appearance of regions of chaos which extend from high $\boldsymbol{\sin\chi}$ across $\boldsymbol{\sin\chi_c}$ allowing classical Q-spoiling of the WG modes. All modes with L_z less than this value to have their Q rapidly degraded. As the Q of these modes decreases it will fall below the threshold Q-value to support lasing and these modes will go dark. But these low L~ modes are the only ones which can emit from the polar regions because of the angular momentum barrier for the high L_z modes. Therefore the model explains naturally why the polar regions are dark while the droplet still lasers. The low L_z modes which could emit from the poles have too low Q to laser and the high Q modes which support lasing are confined away from the polar regions. This argument holds for both the oblate and prelates deformations in agreement with observations.

The question of why the emission profiles are nonetheless so *different* in prelates versus oblate shapes. To answer this question look at where the stable islands which block chaotic escape occur for the two types of deformations. The prelates shape corresponds to a stretching of the droplet in the vertical direction and a compression in the equatorial plane. Because it is compressed in the equatorial plane there exists a large stable island at $\theta = \Pi/2$ corresponding to the two-bounce diametric orbit of the type we discussed in the 2D case .

Ray trajectories

The problems with the proper definition of the term “quantum chaos“ have their origin in the concept of the **trajectory**, which completely loses its significance in quantum mechanics. Only in the semiclassical region do the trajectories eventually reappear, an aspect of immense significance in the context of semiclassical system with N dynamical variables x_1, x_2,…x_N under the influence of an interaction. Typically the x_N comprise all components of the positions and the moment of the particles. Consequently the number of dynamical variables is N = 6M for three dimensional M particle system.

This straightforward generalization of arguments from the circle allows us to define **the decay time** as an average over an ensemble of trajectories on the adiabatic curve $\boldsymbol{p_{m,p}}$, of the time $\boldsymbol{t}$ needed by each orbit to escape. For each orbit, the escape time t can be obtained from a Monte-Carlo simulation, following the classical trajectory and producing at each collision with the boundary a random number between 0 and 1; if the latter is larger than $\boldsymbol{p_o}$, escape occurs.

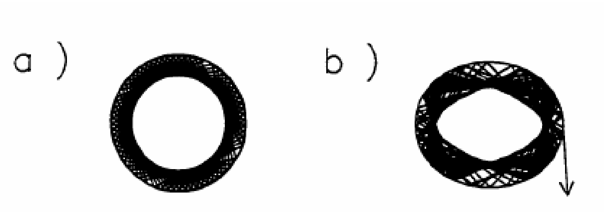

Figure 1.2. Ray trajectories for circle (a), and quadruple-deformed circle (b) parameterized by $r(\phi) = 1 + \varepsilon \cos 2\phi$ in polar coordinates for ϵ = 0.08 corresponding to an 8% fractional deformation. Rays are launched from the boundary at the same Φ and angle of incidence sin χ_0 = 0.7 in both cases; ray escape by refraction occurs in case (b)[21]

The path length. L of the ray up to this event is related to the escape time by $L = ct/n$, and the decay time is

$$\tau = \left\langle \frac{nL}{c} \right\rangle \qquad (1.17)$$

where the average over different trajectories on the adiabatic curve (denoted by the angular brackets) is necessary because $\boldsymbol{\sin\chi}$ is a function of position Φ along this curve, so the starting conditions are in equivalent.

The model thus defined suffers from the approximation that coherence of any kind is not taken into account. This includes the possibility of coherence between successive tunneling events, because the simulation is purely sequential. It also includes the fact that the internal evolution of ***sinχ*** (or ***m***) does not necessarily follow the classical dynamics, e.g. as a consequence of dynamical localization. The only wave effect that is contained in the simulation is direct tunneling through the instantaneous effective potential barrier as derived from the angle of incidence.

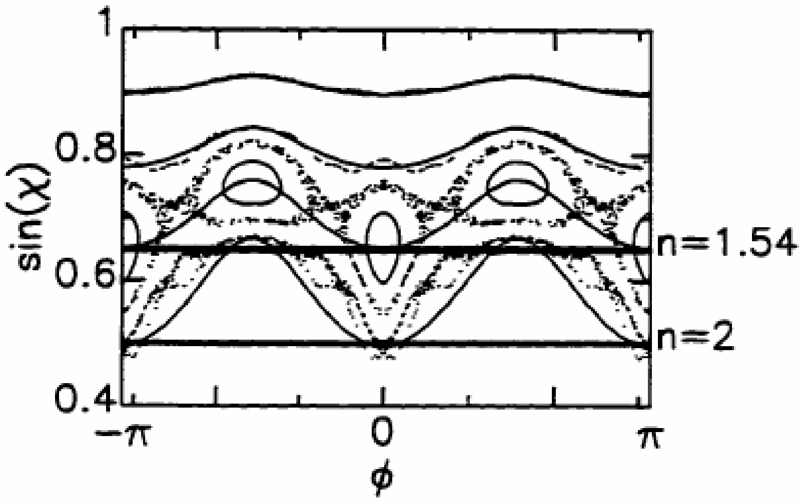

Figure 1.3. The starting condition for the ray escape simulation is given by the adiabatic invariant curve $p_{m,q}$. If tunneling and above-barrier (Fresnel) reflection are neglected, the classical escape condition is that the trajectory cross the line $\sin\chi_c = 1/n$. This defines a billiard with an escape window in phase space that must be reached by classical time evolution. This window is smeared out when the above wave effects are included.[21]

The first of Poincare's integral invariants

$$\oint_C p\,dq \qquad (1.18)$$

where C is the q-space projection of any closed curve in phase space, and all p_i and q, are evaluated at a the same time t.

The quantity in Eq. (1.18) is independent of $\boldsymbol{t}$, even though C will change with **t** according to the equations of motion. To show the invariance of Eq. (1.18), consider each term $\boldsymbol{p.dq_i}$ in the scalar product $\boldsymbol{p.dq}$ separately and apply the integration.

It occurs when a ray starting on the adiabatic curve belonging to a WG mode diffuses downward in $\boldsymbol{sin\chi_c}$ until the condition for total internal reflection

$$\sin\chi > \frac{1}{n} \qquad (1.19)$$

is violated. The real-space picture of this process was illustrated in Fig.1.2, and the location of starting and escape conditions in the Poincare section is shown in Fig.1.3. As an implication of this argument, it is precisely the deviation of the trajectory from the adiabatic curve due to phase-space diffusion that determines the resonance lifetimes at high deformations. This does not constitute a contradiction to the validity of the semiclassical quantization provided the escape times due to classical diffusion are still long enough to permit the adiabatic curve to yield an accurate semiclassical quantization. As a minimal criterion, this calls for at least one revolution around the boundary along the adiabatic curve

Multimode lasing

Lasing requires a gain medium and a cavity. The gain medium provides amplification of a light wave traveling in the cavity, depending on the pump power *P* supplied to it. When *P* exceeds the *lasing threshold* $\boldsymbol{P_t}$, the gain exceeds the losses due to absorption, leakage from the cavity etc. Consider a given cavity mode with a loss rate 1/τ and a number *N* of photons in it. In the limit of a clean resonator, τ is just the resonance lifetime.

To maintain a steady-state laser action, the escape of photons from the cavity must be compensated precisely by the stimulated emission into the same mode. The latter is proportional to the number *Ni* of inverted atoms (or molecules) that interact with the mode, and to the intensity of the existing field. Therefore, can write the stationary condition as

$$0 = \frac{dN}{dt} = BN_i N - \frac{N}{\tau} \qquad (1.20)$$

where *B* is the Einstein coefficient for induced emission.

After canceling *N* we are left with

$$N_i = \frac{1}{B_\tau} \qquad (1.21)$$

which is independent of the pump power. The requirement of steady state therefore implies that the inversion N is *clamped* to a constant value as soon as P exceeds Pt. For the cavities of interest here, one has to assume that many modes have spatial overlap with the gain medium, although their respective τ may vary widely.

After the first mode starts to laser, we could stop increasing P and would thus obtain a single-mode laser. If P grows further, the original mode continues to laser with the same Ni as at threshold ($P = P_t$), but other modes may also satisfy the lasing condition that their modal loss be made up for by their modal gain. This is possible if the spatial overlap of the original mode and the new mode is incomplete, so that one has nodes where the other has antinodes. Since the interaction with the gain medium is suppressed in the neighborhood of field nodes, two such modes can interact with different atoms. The result is that the second mode can indeed laser, producing its own collection of inverted atoms N'_i. Let the threshold for this second mode be $\boldsymbol{P'_t}$. Its loss is larger than that of the first mode $\tau' < \tau$, corresponding to $\boldsymbol{P't > P_t}$. The interesting observation here is that according to

$$\boldsymbol{N'_i > N_i} \quad (1.22)$$

If we add the fact that the amount of pump energy converted into lasing emission grows with the inversion, this leads to the statement that *the lowest-r losing mode carries the largest emission energy.* The same can be said in the presence of more than two lasing modes.

The lasing spectra obtained from liquid spheres and jets containing a dye do indeed show multimode operation. While the longest-lived regular WG states are always among the lasing modes, one can now see how the emission directionality should be dominated by those states whose lifetime is long enough to meet the lasing condition but shortened due to classical escape.

It is then only a matter of achieving the required refractive index before dynamical eclipsing should be seen experimentally. In the absence of a suitable liquid for this purpose, a more immediate goal of an initial experiment is to test the universality of the emission directionality.

Universal directionality

The pseudo classical, and even the classical, model is a good theory for the emission directionality, unaffected by the various approximations that appear to have such a strong effect on the width calculations.

The classical model implies that only the phase space flow near the critical line is of importance for the emission directionality, because the trajectory loses the memory of its starting position during the chaotic diffusion preceding the escape. In the absence of dynamical eclipsing, all that counts is that the tangent adiabatic curve be reached eventually, and the directionality is then prescribed. The same can be said for the flow around the islands if dynamical eclipsing occurs. As a consequence, the emission directionality is expected to be *the same* for all resonances whose semiclassical quantization involves adiabatic curves p_{mq} which are far enough above the critical line for escape.

This is shown in Fig. 1.4 for n = 1.54 where we expect dynamical eclipsing.
The fact that the emission directionality is determined solely by the shape and the refractive index should work in favor of an experimental verification of results. While dynamical eclipsing has not yet been observed, an experiment was recently conducted which confirms the emission from the high curvature points [21].

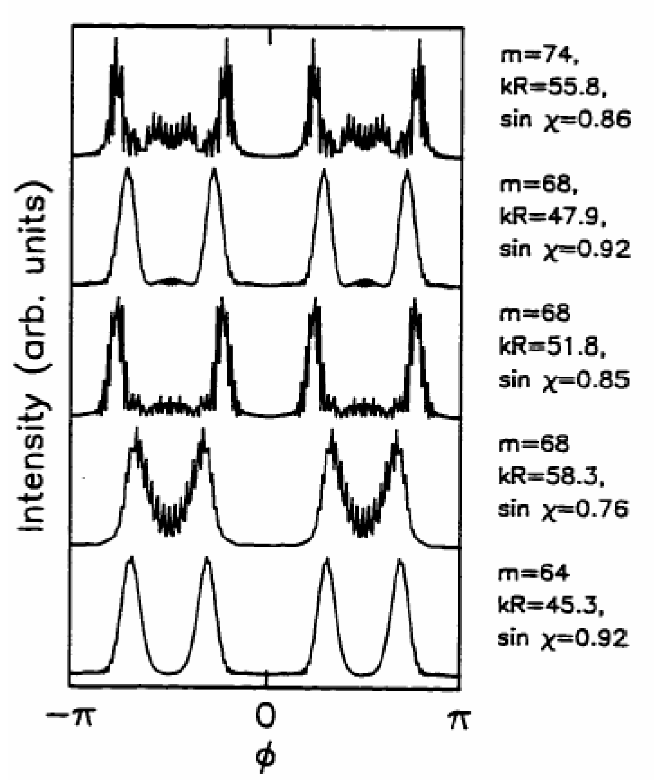

Figure 1.4. Far-field directionality for 5 different resonances of the quadruple at eccentricity e = 0.65 and refractive index n = 1.54, displaying the peak splitting due to dynamical eclipsing.[2]

This was done by creating a cylindrical stream of ethanol containing a lasing dye, which had an oval cross section due to the rectangular orifice at which it was produced. The far-field intensity was found to be peaked, with two maximal in agreement with our discussion above. An observation of importance for device fabrication is that the directionality is also largely independent of deformation beyond some transition region.

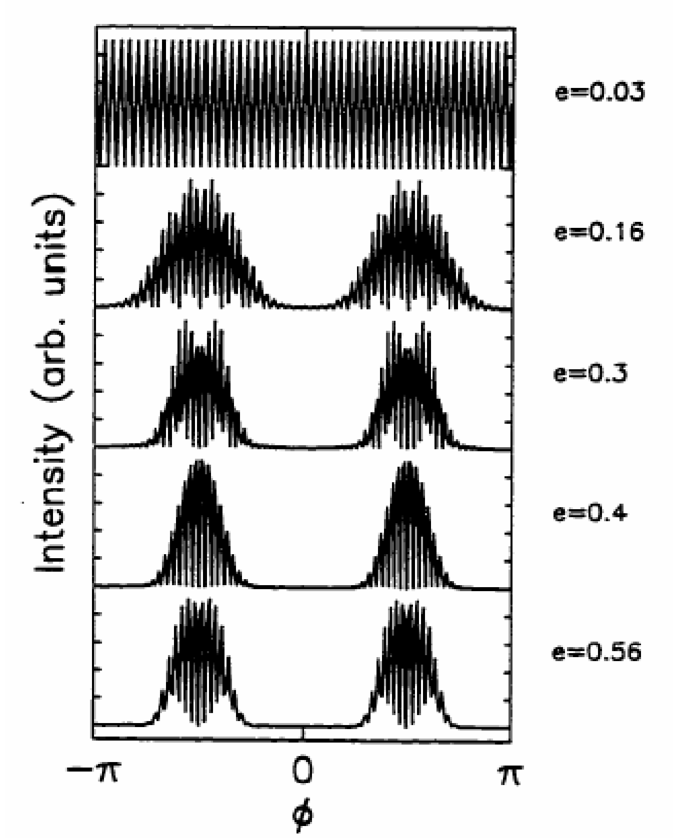

Figure 1.5 . Far-field directionality in the quadruple with increasing eccentricity e at n = 2 for the resonance with m = 45, kR = 27.8 [2]

This is illustrated in Fig.1.5 showing essentially the same intensity distribution above e = 0.3. At e = 0.3, only tunneling escape is possible. As in the ellipse, we still have escape predominantly from the minima of the invariant curve on which the ray moves. The conclusion is that this configuration allows us to tune the resonance *width* over a large interval of practically exponential dependence on e, while the directionality stays unaffected.

In particular, the directionality in the tunneling regime is correctly predicted by the pseudo classical model.
In the case n = 1.54, dynamical eclipsing only occurs after the islands responsible for it have grown to sufficient size. Before that point, the emission looks similar to that of the billiard with n = 2. As shown in Fig.1.6 the four-peak structure has fully developed at e = 0.45, again well before chaotic diffusion becomes possible.

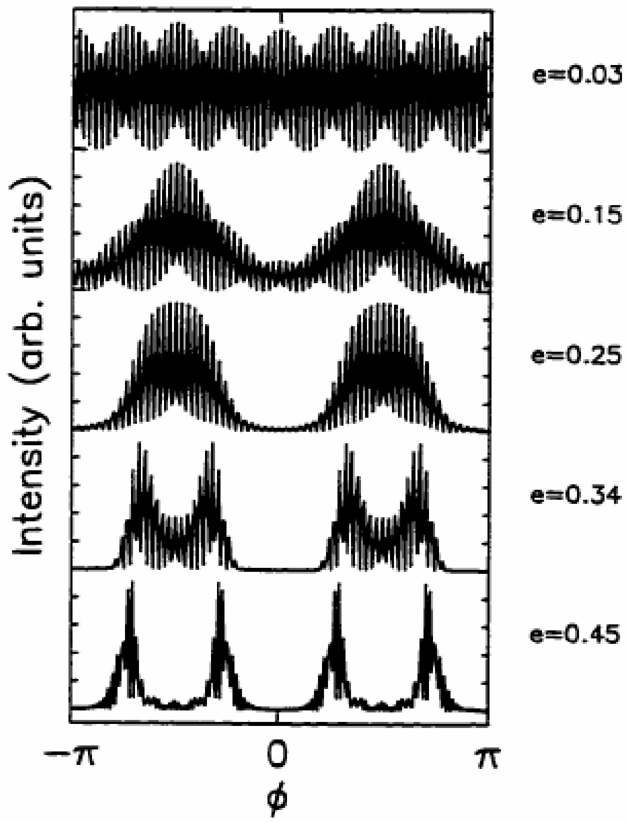

Figure 1.6. Far-field directionality in the quadruple with increasing eccentricity e at n = 1.54 [2]

Emission directionality of quasi-bound states

Whereas up to now the quasi-bound state was introduced only as a convenient tool for extracting resonance widths and positions that could otherwise be determined from Breit-Wigner fits for the scattered intensity. This question was also studied by Young and co-workers [22]. The quasi-bound state can be thought of as the limiting case of a wave packet launched in the cavity and decaying to infinity. An emission process such as lasing, where the light waves are generated in the cavity, rather than being sent in from infinity and then elastically scattered.

If the resonant state is at the complex frequency

$$\omega - i\gamma \equiv c\left(k - ik\right) \qquad (1.23)$$

then the corresponding solution of the time dependent wave equation decays at a rate γ since it has the form

$$\psi(r,t) = \psi(r)e^{-i\omega t}e^{-\gamma t} \qquad (1.24)$$

where $\gamma > 0$. But as a function of r, the outgoing waves in fact exhibit exponential growth because

$$H_m^{(1)}(x) \approx \sqrt{\frac{2}{\pi x}}e^{i(x-m\pi/2-\pi/4)} \qquad (1.25)$$

for large values of ***x = (k—ik)r*** . The physical reason for this growth with e^{kr} is a retardation effect: the field at r >> *R* has propagated away from the cavity where it originated a time $\Delta t = r/c$ in the past - but at that earlier time the field at the cavity was larger by a factor $e^{-\gamma\Delta t.}$

As can be seen from Eq. (1.25), all the Hankel functions in the outgoing wave depend on r through the *same* factor $\sqrt{\frac{2}{\pi x}}e^{i(k-ik)r}$ in the far-field (r >> *R)*. Pulling out this common dependence, the field of the quasibound state factorizes into radial and angular functions,

$$\psi(r) = \sqrt{\frac{2}{\pi x}}e^{i(k-ik)r}E(\phi) \qquad (1.26)$$

This means that the directionality at large distances becomes independent of r, being contained solely in *Ψ(Φ)*. Chosen r in this far-field region and plot the square of the electric field (which is proportional to the intensity) as a function of *Φ* to obtain the wave directionality.

Also note that the above-mentioned exponential growth does not show up in this figure. This is clear from Eq. (1.26), which tells us that due to the prefatory the wave function will in fact fall off up to a distance r = l/(2k), and only beyond this r begin to grow. Since κR < 1/10 as will be seen later, the figure captures only the spatial decay. This emission process differs from elastic scattering which requires an incoming wave to excite the resonance. The directionality pattern in a scattering experiment will depend on the form of the incident wave both because of interference with the outgoing wave, and because the incident wave may couple preferentially to different senses of circulation of the rays. These effects are absent in emission, so a unique directionality profile will be observed that depends only on the quasibound state itself and should be approximately described by our ray optics model if *kR* is sufficiently large.

Whispering gallery modes WG

Whispering gallery modes and their ultrahigh cavity quality *Q* factors of circular micro cavities can be associated with regular ray dynamics in the cavities.

If the interface can be made clean and smooth, the only leakage out of such a cavity stems from the fact that the surface has a finite curvature so that total internal reflection is violated, allowing a small fraction of the internal intensity to escape. This mechanism is closely related to quantum mechanical tunneling, and the escape rates are correspondingly small. Consequently, we will study the particular class of resonators characterized by a (not necessarily small) deformation which, however preserves convexity everywhere along the boundary. We call this class **asymmetric resonant cavities** (ARCs). Asymmetric resonant cavities hold great promise as the **Kolmogorov-ArnoPd-Moser (KAM)** theorem of Hamiltonian classical mechanics experimental systems. The results that are obtained for whispering gallery modes in simple convex but strongly asymmetric resonant cavities can be summarized as follows:

Red shift: The resonance frequency always shifts to lower values with increasing deformation when constant area is maintained. This can be explained using an adiabatic approximation based on the proximity to the boundary and hence to Lazutkiirs caustics.

Broadening: The resonance lifetime, r, always decreases with deformation. For each resonance, there is a classical threshold deformation beyond which its lifetime is dominated by classical ray escape as opposed to tunneling (i.e. the small violation of total internal reflection present even in the circle).

At such large deformations, ***r*** becomes independent of frequency provided ***a***; is large enough. The *universal* resonance broadening depends only on the index of refraction and the angle of incidence characterizing the whispering gallery orbits.

Directionality: Emission from a quasibound state is highly anisotropic at strong deformations, with intensity peaks in directions that are determined to high accuracy by the phase space structure of the classical ray dynamics inside the cavity. At deformations high enough for classical escape to dominate over tunneling, the directionality is furthermore *universal* for all whispering gallery resonances, and the only parameter that affects it is the refractive index.

In the circle, we know that whispering-gallery WG resonances are narrow due to the low tunneling escape rate. The basic idea that opens the connection to nonlinear dynamics is that at sufficiently large deformations, a new and competing escape mechanism becomes dominant, replacing tunneling as the process limiting the decay. The resonance lifetime at high deformation is limited by *classical ray escape*.

The **Husimi distribution** is a Gaussian smoothed version of the Wigner function, representing the corresponding quantum mechanical probability distribution in phase space [4]. Husimi distribution has significant overlap with the region below the critical angle and thus the output directionality is mainly determined by the intracavity mode distribution as usual [3]. In addition, for high-Q modes for rather small nka, namely □ 50, which happens to be the size parameter at which many o ther theoretical studies have been performed on the role of unstable manifolds in output directionality [4], the faint structure corresponding to the unstable manifolds has not been observed in numerical studies [3].

The evident importance of the system’s underlying classical phase space for the behavior of the quantum or wave mechanical analogue (based on the analogy between Schr¨odinger and Helmholtz equation [1]), its specific structure cannot be reconstructed from the traces it leaves in typical observables like energy level or wave function statistics.

Recently predicted **super scars** have been identified experimentally and using the well-known analogy between the electric field strength and the quantum mechanical wave function in a two-dimensional microwave billiard their properties determined

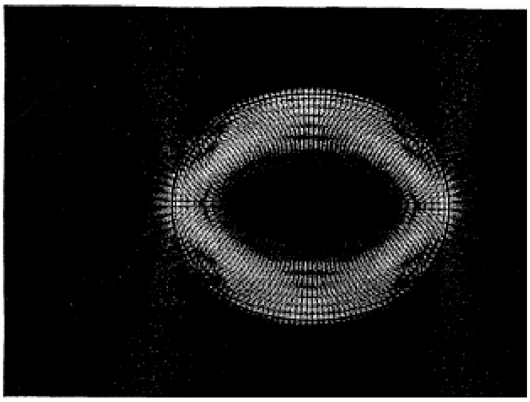

Figure 1.7. Scarred light distribution in a distorted glass fiber cavity [1]

To establish some experience with the phenomenology of the chaotic transition in billiards, it is instructive to discuss . These will subsequently be used both in classical and wave mechanical calculations. Only convex deformations of the circle are of interest to us, because that is the requirement for the existence of whispering gallery orbits.

To compare different shapes among each other, a measure of the deformation is required.

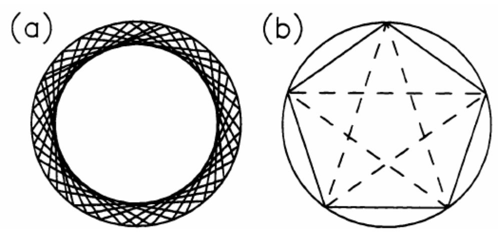

Figure 1.8. (a) A typical quasiperiodic trajectory in the circular billiard
(b) Five- bounce periodic orbits [1]

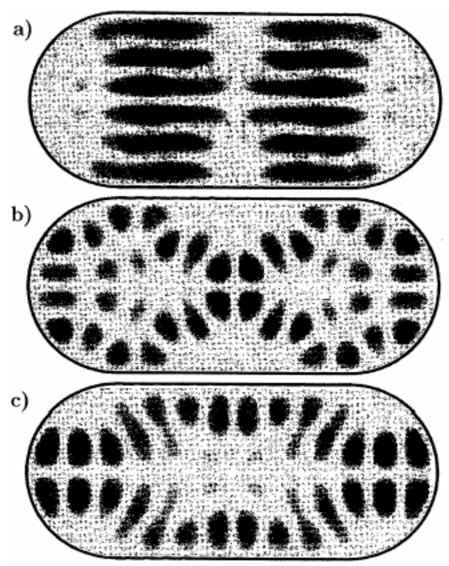

Figure 1.9. Experimental eigenfunstions in a microwave resonator of shape of a stadium billiard. For the display of the wave functions the stadium has been completed by a twofold reflection. All wave functions show strong scarring close to classical periodic orbits.[1]

Avoided crossing

Eigenvalues of these quantum systems generally exhibit repulsive interaction. This interaction comes from an absence of conserved quantities other than energy in the corresponding classical systems, and gives rise to ***avoided crossings*** when a parameter of the Hamiltonian is varied. These features have been studied by the use of eigenvalue statistics such as the nearest-neighbor spacing distribution and the spectral rigidity [5-7]

We can see that the characteristics of eigenfunctions alternate between two levels when the parameter goes through an avoided crossing. At an avoided crossing, eigenfunctions do not exhibit clear characteristics of scars. From the above observation, we can generally expect that invariant characteristics corresponding to scars continuously change along the diabetic transition lines rather than along the adiabatic level lines.

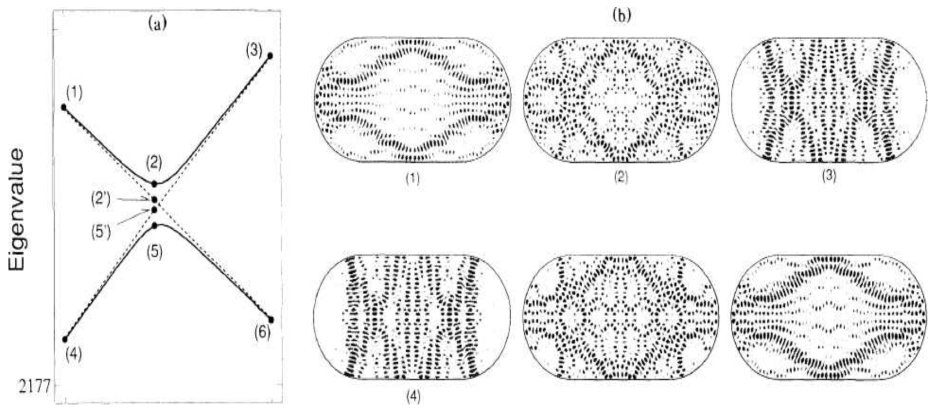

Figure 1.10. (a) Eigenvalues of stadium billiard under variation of the aspect ratio λ as a parameter (solid line), and diagonal elements, a(λ) and b(λ), in the diabetic representation (dotted line); (b) squared absolute value of eigenfunctions around the avoided crossing. These are the 289th and 290th states in the antisymmetric subspace of stadium billiard having the area π+4 [4]

The relation between diabetic transformation and periodic orbits can be seen through Fourier transformation of the level density

$$\tilde{d}\left(x\right) \equiv \int_0^{k_N} dk \exp\left(ikx\right) \sum_{j=1}^{\infty} \delta\left(k^2 - k_j^2\right) \equiv \sum_{j=1}^{N} \frac{\exp\left(ik_j x\right)}{2k_j} \qquad (1.27)$$

where k^2_j is a value of the j$^{\text{th}}$ energy level.

Microcavity laser

The prototypical optical system that spurred our interest is the which has been realized experimentally both in liquid droplets with a lasing dye. Conventionally, one uses Bragg reflectors to provide Fabry-Perot type mode confinement, but this does not lead to quantization of all degrees of freedom, and one faces limitations in the feasibility of fabricating small devices. The reason is that the Bragg reflectors then become large in relation to the actual cavity.

The microcavity lasers do not require Bragg reflectors at all. They make use of modes propagating inside a dielectric close to the interface with the air outside. These modes correspond to rays traveling around the perimeter, confined to the dielectric by total internal reflection at the interface.

The study of classical periodic orbits can be a good starting point in fully chaotic systems because of the following three reasons.

- The first is that periodic orbits are known to correspond to energy levels in the semiclassical limit. This correspondence is given by Gutzwiller's trace formula,

$$\sum_j \frac{1}{E-E_j} \approx -\frac{i}{\hbar} \sum_{periodic-orbits} \frac{T_0}{2\sinh\left(\alpha/2\right)} \times \exp\left[\frac{i}{\hbar} s - il\frac{\pi}{2}\right] \quad (1.28)$$

where $\boldsymbol{T_o}$ is the period of a classical orbit, $\boldsymbol{S}$ is the action integral along it, / is the Maslov index, and $\boldsymbol{a}$ is determined from the stability of the orbit. According to this formula, the Fourier transformation of the level density is expected to have peaks at each length of the periodic orbit with a height corresponding to the stability of it [8].

- The second reason is the existence of *scar* eigenfunctions [9,10]. This clearly shows that each eigenstate can be a *superposition* of a few classical periodic orbits. We expect that eigenstates can be characterized by classical periodic orbits for chaotic systems in place of tori for integrable systems.

- The third reason is that, in fully chaotic systems, periodic orbits densely exist in phase space because of the ergodicity. Although they are isolated, they can play a role in coupling quantum states because of the finite *h*.

Deformed Microcavity (DMC)

Besides advantage properties to investigate the chaotic system similar a microcavity as compact size, high Q-factor, ..a deformed microcavity also has

- Directional emission.

- High - Pumping efficiency (no resonant case)

- Chaotic ray dynamic (basis of wave chaos)

We have chose the liquid micro jet DMC is a tool for studying ray and wave chaos. The properties of micro cavity highly depend on the degree of deformation.. If one can tune the deformation of a micro cavity from a perfect circle to a final deformed form continuously, one can follow the evolution of modes and thus can easily identify the origin and mode numbers of observed modes of DMC. Such identification allows us to perform direct comparison with wave calculation and helps us obtain better understanding on the connection between the mode distribution, cavity quality factors and output directionality of these modes, and the aforementioned chaotic ray dynamics.

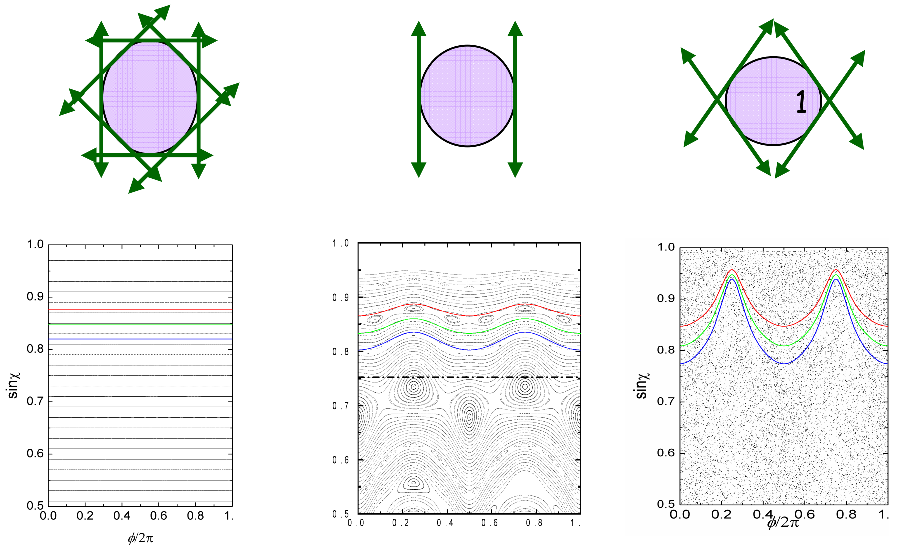

Figure 1.9. Directional and Chaotic ray dynamic in some micro cavity.[16]

Actually, we can control of the degree of deformation and thus we can follow a mode evolution continuously. While the Direction of lasing emission is different and Q - values are tunable by the degree of deformation.

Quadruple micro cavity (QMC)

The boundary is parameterized in polar coordinates by

$$r(\phi) = \frac{1}{\sqrt{1+\varepsilon^2/2}}(1+\varepsilon\cos 2\phi) \qquad (1.29)$$

The area of this domain is π. All other deformations will have as their dominant multimode component this term, and we can therefore use the strength of the quadruple part as a measure of the deformation that allows a comparison between different shapes

The output directionality observed from deformed micro cavities has been explained either by ray dynamics based on chaos theory [1], or by the nature of modes obtained from Maxwell's wave equations. Adequacy of each approach depends on several factors, but most importantly on the size of micro cavity with respect to the wavelength of interest or the size parameter nkr, where n is the refractive index of the cavity medium, k - the wave vector with λ the wavelength and r the representative radius of the cavity.

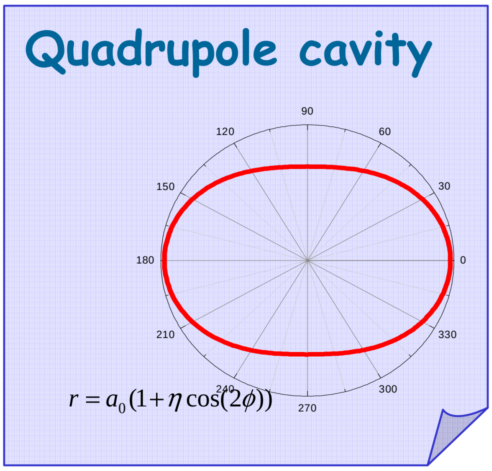

Figure 1.10. A quadruple deformed microcavity.

Its component is more than 97% [16]

Since the damping constant of some DMC, we see that after 39 μs (period of oscillation) only quadruple shape remains: No movable points are characteristics of only a quadruple.

$$r = a_0(1+\eta_2\cos 2(\phi+\varphi_2)+\eta_3\cos 3(\phi+\varphi_3)+\eta_4\cos 4(\phi+\varphi_4)+\cdots) \quad (1.30)$$

2. Experiment

In principle

We have developed a technique for realizing a two dimensional quadruple micro cavity with its deformation variable from 0% to 20 % continuously using a liquid jet ejected from noncircular orifice. With this technique, we investigated the far field evolution depending on deformation parameter from regularity to chaos.

The Liquid jet micro cavity is the most suitable to study fully chaotic systems because of the following three reasons

- Ultra high Q-value, small size and clear boundary shape is possible due to the smoothness of surface by surface tension.

- The degree of deformation is continuously tunable.

- It is easy to control the concentration of gain material

The micro jet is excited by an argon-ion pump laser at 514 m. The pump laser is focused with a cylindrical lens into a thin profile with a thickness of 10 μm in the *z* direction so that a thin slab can be selected to be a two-dimensional micro cavity in the micro jet. The fluorescence emitted from this region is collected by an objective lens and delivered to a spectrometer with a charge-coupled-device detector.

An DMC can be obtained from a horizontal cross section of a micro jet, which is made of ethanol n=1.361 doped with Rhodamine B dyes as gain molecules. The cavity-modified fluorescence (CMF) or lasing light from the QDM is collected by an objective lens with a full collection angle of 5 degrees and focused on to an entrance slit of a spectrometer.

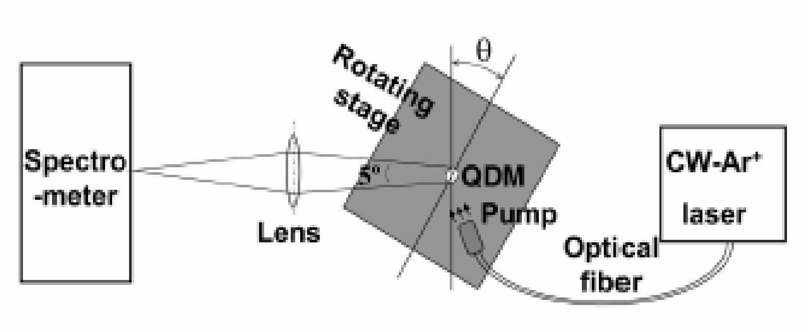

Figure 2.1. Schematic of our experimental setup for measuring cavity mode spectrum and single-mode far-field emission pattern of a QDM.[11]

The fabricating process of deformed orifices

The shape of the jet column can be approximated in the cylindrical coordinates by the following time independent equation

$$r_{t,z} = \left[1 + \eta_0 \exp\left(-\frac{z}{v_z \tau} \sin\left(\frac{2\pi}{v_z \tau} z + \xi \right) \cos 2\theta \right) \right] \qquad (2.1)$$

where a is the mean radius, η is a deformation parameter, τ is the decay rate, T is the period of oscillation, and ξ is an initial phase of oscillation. The jet velocity v_z is assumed to be uniform across the entire jet

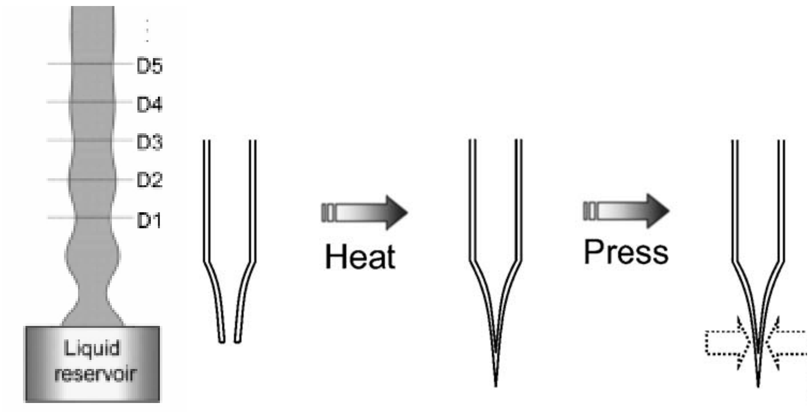

Figure 2.2. a. Model for the deformed microjet column.
b. Fabrication procedure of a noncircular orifice.
The side view shows that the inner walls are inclined. [11,16]

From Eq.1.29, the micro jet boundary at the nozzle z=0 is

$$r(\theta, z_n) = a\left[1 + (-)^n\right]\eta_n \cos 2\theta \qquad (2.2)$$

The tip of a Pyrex tube is placed vertically in the center of a Nichrome heating coil. The bottom of the orifices are melted, narrowed and inclined, resembling the letter "V,". The tip are pressed with a tweezers to desire deformation. The end of cut back and polish them to control their dimension. Gradient about vertical axis play a critical role in tuning of deformation

A noncircular orifice induces a micro jet to form a stationary tidal column as depicted in Fig.2.2 – 2-5, the micro jet surface becomes well approximated by Eq. 2.2 demonstrate a horizontal cross section of a micro jet or antinodes planes at z_n as Dn (n=1,2,3,…). We made orifices a different deformation.

Obtain a deformed microcavity

Due to surface tension, the liquid jet ejected from the deformed orifice exhibits shape oscillation as it is launched upward.

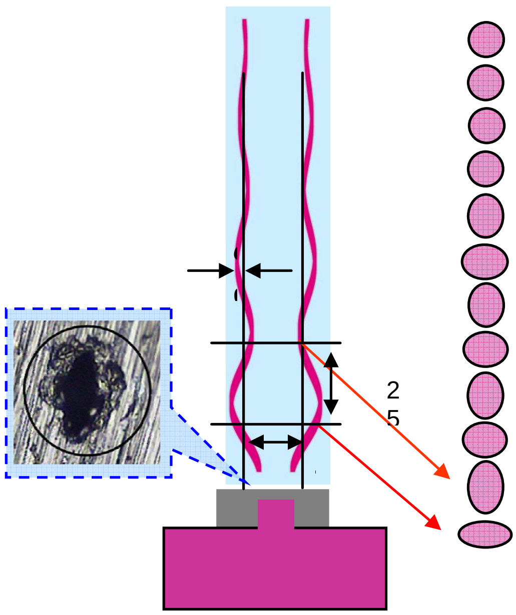

Figure 2.3. Obtain the shape oscillation from the deformed microcavity
The left view is a real image of a noncircular orifice [16]

A two-dimensional asymmetric resonant cavities (ARC), specifically a quadruple deformed micro cavity (QDM), is obtained by selecting cross- sectional planes located at the extreme z_n's (n =−1,0,1,2,...) in Fig.2.2 (a) of the amplitude oscillation, where the cavity boundary is given by Eq.2.2

The degree of possible three-dimensional (3D) effect due to a finite thickness of the region to be used in experiment around the cross- sectional plane, which is about 10µm, can be estimated in the following way. Under our experimental conditions to be described below, a typical value of $v_z T$ is 280µm, which is much larger than the mean radius a of 15µm. The possible variation in the cavity size over the 10µm region in the z direction is then estimated to be less than 0.1% or 0.02 µm in diameter, and therefore the 3D effect can be safely neglected.

Control the degree of deformation

In principle, when has been ejection pressure change, radial velocity of jet change and correspondingly initial degree of deformation change

From η_0 can deformation tuning at antinodes planes by the jet ejection pressure. Fo r example, with an ejection pressure increased to 2.0 bars, we obtained a new set of QDM's with deformations of 29,8 % (D1), 20,4 % (D2), 14,5 % (D3), 10,6 % (D4), 7,5 % (D5),5,0 %(D6) etc., increased from 22,4 % (D1), 16,9 % (D2), 12,6 % (D3), 8,5 %(D4), 5,5 % (D5), 4,3 % (D6), etc. at 1.8 bars. (Fig. 2.4)

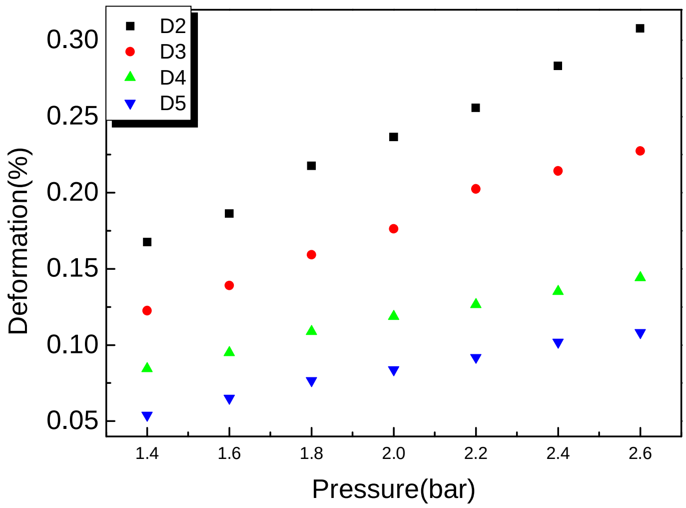

Figure 2.4. Variation of deformation parameter according to the ejection pressure of the jet at D2–D5 positions.[16]

The pinching of the nozzle in one direction in the fabrication process has introduced different inner wall slopes, and these different wall slopes in turn induce different initial radial velocities, which makes it possible to tune the cavity deformation. We then obtain the following result showing that the seed deformation can be controlled by the jet ejection velocity

$$\eta_0 = \sqrt{\eta_i^2 + \left(\frac{KT}{2\pi a}\right)^2 v_z^2} \qquad (2.3)$$

Due to the gradient about vertical axis, jet flow out with initial radial velocity and the initial deformation increase by initial radial velocity.

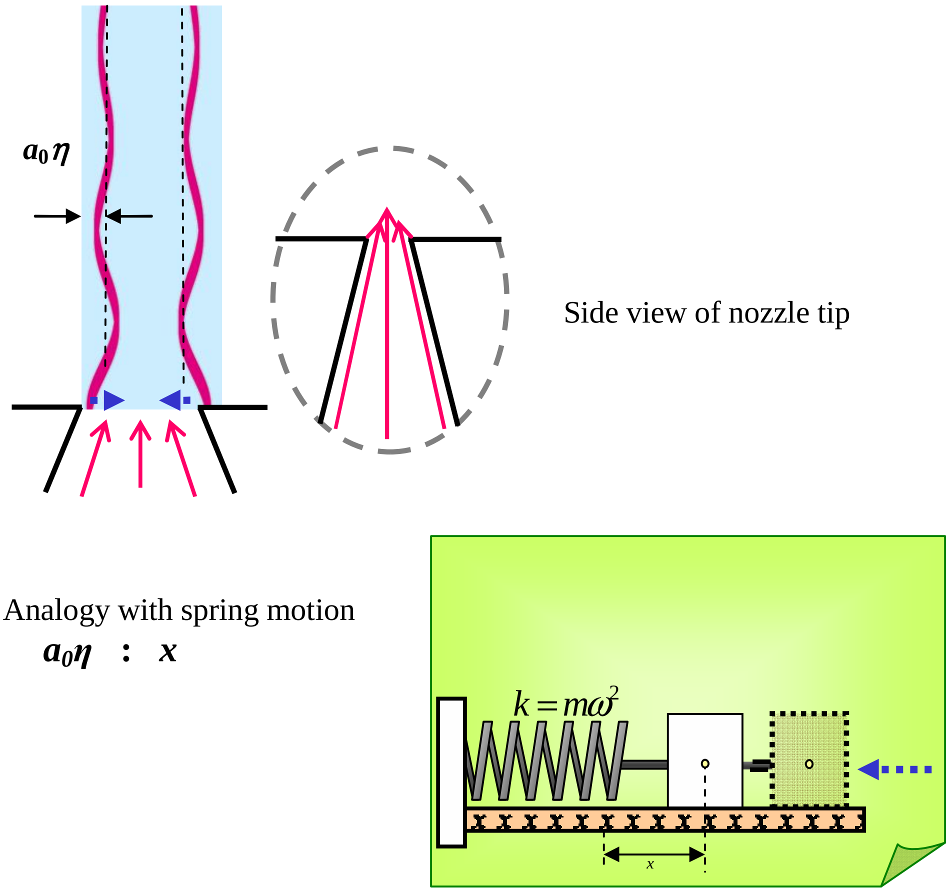

Figure 2.5. Principle schematic of Controlling the degree of deformation [16]

The jet ejection velocity is easily controlled by the ejection pressure. It is noted that the oscillation of the quadruple deformation along the $\boldsymbol{z}$ direction is analogous to a damped harmonic oscillator with a nonzero launching velocity. The dependence of ε and consequently the amplitude of deformation oscillation on the jet velocity v_z are illustrated in Fig.2.5. In addition, the contribution due to the damping in the initial radial velocity is much smaller than that of the harmonic oscillation.

Measure the degree of deformation from diffraction pattern

The degree of deformation of QDM's can be determined from their diffraction patterns made by an incident Ar laser. The deformation parameters measured by the diffraction technique as in Figure 2.6. The degrees of deformation of QDM's are found to be :

29,8% (D1), 20 % (D2), 14,5 % (D3), 10,6 % (D4), 7,5 % (D5), 5.0 %(D6), etc. under **1.8 bars** of ejection pressure.

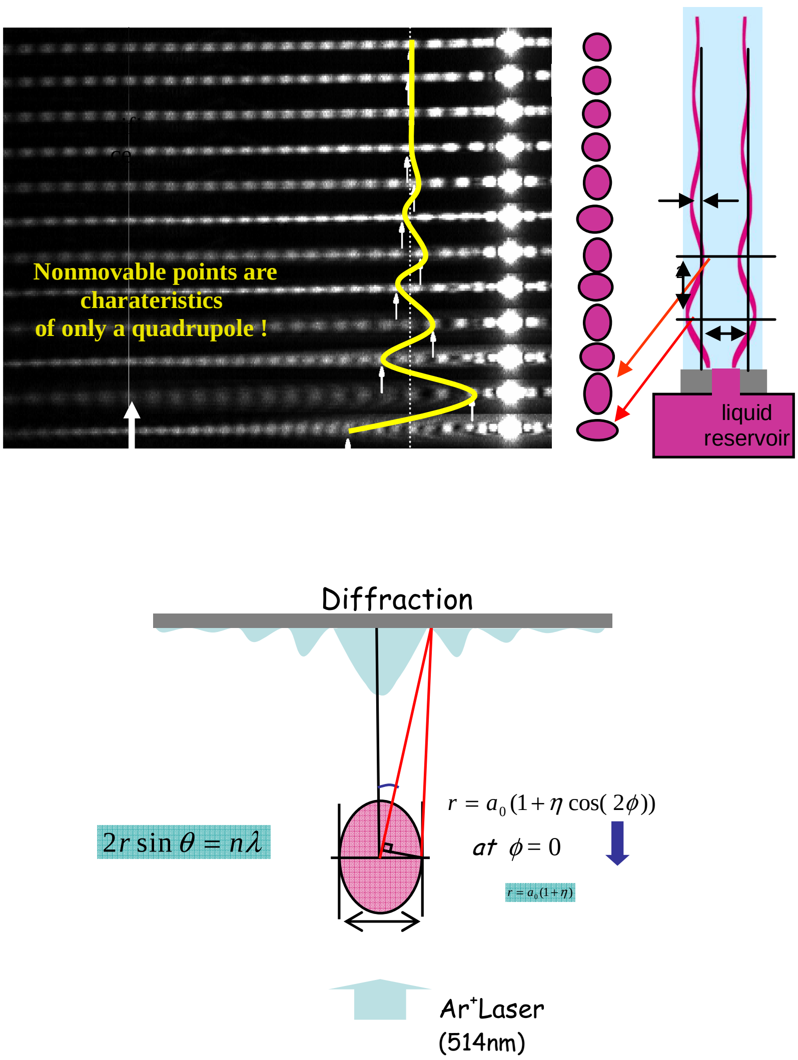

Figure 2.6. Measure the degree of deformation from diffraction pattern [16]

Obtain the evolution of lasing directionality

One of the behaviors to reach studying the quantum states is to consider them at the boundary of classical mechanics whereas the applicability of classical mechanics theory. Therefore the principle to build a deformed micro cavity for research quantum properties in chaos medium to elucidate the interplay between wave and particle natures of light.

The output directionality observed fro deformed micro cavities has been explained either by ray dynamics based on chaos theory [1], or by the nature of modes obtained from Maxwell's wave equations. Adequacy of each approach depends on several factors, but most importantly on the size of micro cavity with respect to the wavelength of interest or the size parameter ***nka***, where ***n*** is the refractive index of the cavity medium, k= 2π/λ- the wave vector with the wavelength and ***a*** the representative radius of the cavity. Since the off-resonance pumping efficiency for a QDM depends on pumping angle [12], the pump laser beam is delivered through an optical fiber with its exit end mounted on the rotatable stage with a fixed angle of 45◦ with respect to the major axis of QDM when output spectrum and directionality are measured. The cavity-modified fluorescence (CMF)or lasing light from the QDM is collected by an objective lens with a full collection angle o f 5 degrees and focused on to an entrance slit of a spectrometer. A polarizer pl aced in front of the slit selects only the polarization component parallel to the QD M column. The emission spectrum is then measured for a fixed angle ***θ*** of the r otation stage (Figure 2.7)

The size parameter ***nka*** have a important role to choose the regime whereas mode formation in the cavity. In other words, let's find what its value corresponding to an interesting regime where wave and particle nature of light may coexis.

With ***nka*** large , the fact that the free spectral range (FSR) of a mode in such large cavities is not much larger than the line widths of individual modes of relatively low cavity quality factor Q, associated with the observed output directionality. Actually, properly chosen size parameter ***nka~200*** due to limitation in numerical computation and due evidently the various modes observed in this case, to elucidate the interplay between wave and particle natures of light in DMC [11].

A hint comes from the observation that the far-field emission pattern obtained from ray dynamics in classical limit for the QDM is similar to those from the wave calculation and the experiment. For an open system, long time ray dynamics in chaotic region are predominantly determined by the so-called unstable manifo lds [2, 3].

As the deformation is increased gradually, this dynamical regularity begins to be broken following the Kolmogorov-Arnold-Moser (KAM) scenario in phase space.

The emission pattern also experiences a dramatic change from isotropic emission to collimated tangential emission at high-curvature points on the surface. When the deformation is further increased, even KAM tori are broken and the internal ray dynamics becomes more chaotic.

These universal directionality of high Q modes can be explained by unexpected manifestation of particle nature of light or ray flow in classical chaos in the formation of quasi-bound states in quantum chaos, corresponding to the wave nature of light.

By background luminescence, mostly due to bulk fluorescence of the cavity medium, can be discriminated. The resulting single-mode far-field emission pattern is shown in Fig.2.7. In comparison, previously reported far-field patterns for deformed micro cavities of nka□10^3 [3] were measure without any resolution on individual modes and thus they correspond to multimode far-field emission patterns.

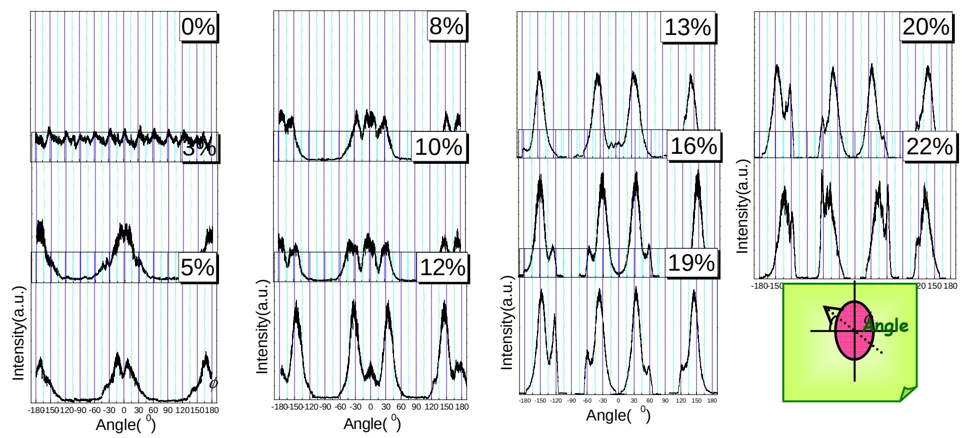

Figure 2.7. The emission directionalities seen in the far-field distribution show the transition of mode dynamics from regularity (0%) to chaos (22%).
Emission properties : at 0 % : Isotropic emission,
at 5 % : Tangential emission at high curvature,
at 16 % : Highly directional emission [16]

Since rays escapes from an open cavity before reaching complete lyer geodic limi t, ray dynamics is usually restricted in limited phase space and thus follows a few dominant unstable manifolds.

We observed the evolution of lasing directionality from deformation parameter 0% (regularity) to 22% (chaos) in Figure 2.7. This result has compared with calculated wave function in figure 2.8. They are represented the correspondence with each other.

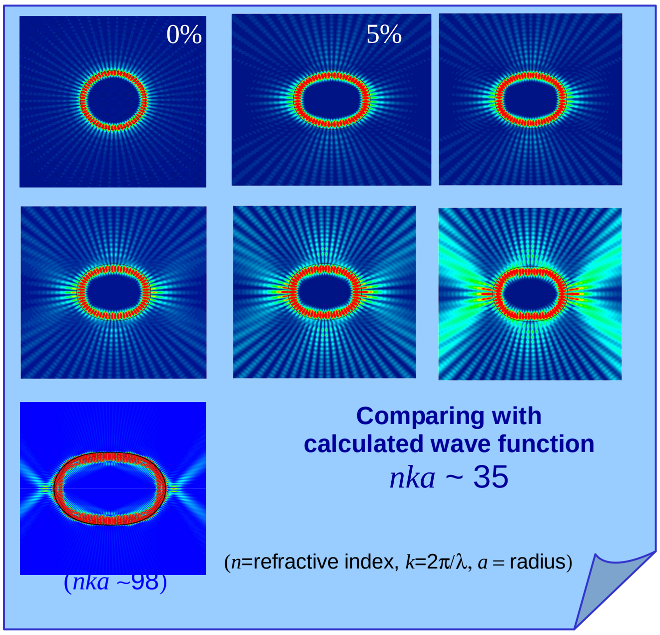

Figure 2.8. Results from calculated wave function with ***nka ~ 35*** [16]

Conclusion

Above experiment results have elucidated basics of quantum chaos theory in Session I. Clearly, the deformed micro cavity is an efficient tool to study quantum chaos phenomena, which essential high complicated. The fabricating of deformed orifices is successful and its parameters chosen appropriately obtained interesting results. In the future we hope from that DMC will obtain complicated spectra for avoided crossing effect as well as its deferent interesting effects.

References

[1] Hans-Jurgen Stockmann “Quantum chaos” (Cambridge University, 1999).

[2] J. U. Nockel and A. D. Stone, *Optical Processes in Microcavities*, edited by R. K. Chang and A. J. Campillo (World Scientific, Singapore, 1996).

[3] J.B.Shim et al.,“Regular spectra and universal directionality of emitted radiation from a quadruplar deformed microcavity”, arxiv.org/abs/physic /0603221.

[4] H. G. Schwefel et al., J. Opt. Soc. Am. B 21, 923 (2004)

[5] O.Bohigas and M.J.Giannoni, in Matematical and Computational Methods in Nuclear Physics, edited by J.S.Dehesa, J.M.G..Gomer, and A.Polls, Lecture Notes in Physics Vol.209 (Springer, Berlin, 1984), p.1.

[6] M.V.Berry, in Chaotic Behavior of Deterministic Systems, Proceedings of the Les Huches Summer School, Session XXXVI edited by G..Iooss, R.H..G..Hellman

[7] M.Wilkinson, J. Phys. A20, 635 (1987); 22, 2795 (1989)

[8] D.Wintgen, Phys. Rev.Lett. 58, 1589 (1987); A.Shudo and Y. Shimizu, Phys. Rev. A42, 6264 (1990)

[9] E.J.Heller, Phys.Rev.Lett. 53, 1515 (1984)

[10] M.Feingold, R.G. Littlejohn, S.B.Solina, and J.S.Pehling, Phys. Lett. A146, 4 (1990)

[11] S. B. Lee et al., Phys. Rev. Lett. 88, 033903 (2002).

[12] J. Yang et al.,“Development of deformation-tuable quadrupolar microcavities”, arxiv.org/abs/physics/0603247.

[13] L. E. Reichl, The Transition to Chaos in Conservative Classical Systems: Quantum Manifestations (Springer- Verlag, New York, 1992).

[14] A. J. Lichtenberg and M. A. Lieberman, Regular and Stochastic Motion (Springer-Verlag, New York, 1983).

[15] Toshiya Takami, Phys. Rev. Lett. Vol 68, 23 (1992)

[16] S. B. Lee, J. Yang, T.T.A.Dao et al ” Observation of the far field evolution in a shape-variable microcavity”, **TP-I1,** OSK, Sokcho, July 18-20, 2007

[17] M.C.Gutzwiller. Chao in Classical and Quantum Mechanics. Springer- Verlag New York 1990

[18] T.Guhr,A.Muller-Groeling. Random matrix theories in quantum physics. Phys.Rev. 299,189 (1998)

[19] V. I. ArnoFd, *Mathematical Methods of Classical Mechanics* (Springer, New York, 1989)

[20] P. J. Richens and M. V. Berry, Physica 2D, 495 (1981)

[21] J. U. Nockel, A. D. Stone, G. Chen, H. Grossman and *R.* K. Chang, Opt. Lett. 21, 1609 (1996)

[22] E.S.C.Ching, P.T. Leung and K. Young, *Optical Processes in Microcavities*, R. K. Chang and A. J. Campillo, eds., (World Scientific, Singapore, 1996)